



Cite this: *J. Mater. Chem. C*, 2016, 4, 4939

## Low mid-infrared absorption tolane liquid crystals terminated by 2,2-difluorovinyl: synthesis, characterization and properties†

Minggang Hu,<sup>abc</sup> Zhongwei An,<sup>\*ab</sup> Jian Li,<sup>ab</sup> Haiwei Chen,<sup>c</sup> Fenglin Peng,<sup>c</sup> Shin-Tson Wu,<sup>c</sup> Xiangru Wang<sup>d</sup> and Man Li<sup>e</sup>

The synthesis and characterization of new 2,2-difluorovinyl terminated tolane liquid crystals are reported. The mesomorphic properties, mid-wave infrared (MWIR) absorption and birefringence were investigated. The results show that these materials exhibit low absorption loss, a wide nematic phase range, a low melting point and high birefringence. The influences of fluorine substitution and terminal groups were discussed. Moreover, a room temperature eutectic mixture is formulated with relatively high birefringence ( $\Delta n = 0.254$  at  $\lambda = 4 \mu\text{m}$ ), modest dielectric anisotropy ( $\Delta\epsilon = 2.37$ ), low viscosity (182.9 mPa s) and a low absorption coefficient in the 3–5  $\mu\text{m}$  region.

Received 26th March 2016,  
Accepted 19th April 2016

DOI: 10.1039/c6tc01249c

www.rsc.org/MaterialsC

### Introduction

In addition to displays, liquid crystals (LCs) have also found useful applications in many photonic devices in the visible,<sup>1,2</sup> infrared (IR),<sup>3,4</sup> millimeter wave,<sup>5,6</sup> and terahertz spectral regions.<sup>7,8</sup> In particular, the mid-wave infrared (MWIR,  $\lambda = 3\text{--}5 \mu\text{m}$ ) band represents a strategically important spectral region for photonic sensing,<sup>9,10</sup> communication,<sup>11</sup> spectroscopy,<sup>12</sup> etc. The use of LC devices in the MWIR region offers some attractive features, such as high performance, low cost, compactness and lightweight, low power consumption, and good reliability.<sup>13</sup> High birefringence LCs in the MWIR region<sup>14</sup> have been used in laser beam steering,<sup>15</sup> adaptive optics,<sup>16</sup> Lyot filters,<sup>17</sup> light shutters<sup>18</sup> and photonic crystal fibers.<sup>19</sup>

The molecular design strategies for visible displays and IR phase modulators are quite different. In particular, for MWIR applications, besides a wide nematic temperature range, high birefringence and low viscosity, low absorption is another critical requirement. A good balance between physical properties and MWIR loss should be considered. LCs with high birefringence have been studied for potential IR applications, such as

cyanotolanes and cyanostilbenes,<sup>20</sup> cyanobiphenyls,<sup>21</sup> diazo liquid crystals,<sup>22</sup> and bistolanes.<sup>23,24</sup> However, a major challenge in using these LCs in the MWIR region is large absorption loss.<sup>20,21</sup> The absorbed light will convert into thermal energy, which affects the birefringence and viscoelastic constant and even causes the light modulation capability to vanish completely while the temperature is over the LC's clearing point.<sup>25</sup>

Several inherent molecular vibration bands exist in the MWIR region, such as CH, CH<sub>2</sub>, and CH<sub>3</sub>, exhibiting strong and broad absorption from 3.2 to 3.7  $\mu\text{m}$ , the cyano (CN) absorption peak occurs at  $\sim 4.48 \mu\text{m}$  and isothiocyanato (NCS) has a broad and strong absorption in the 4.5–5.2  $\mu\text{m}$  spectral region. Therefore, CN and NCS should be replaced by F or Cl as a polar group. The C–H bonds in the alkyl chain or in the aromatic rings are basic elements for an organic compound to exhibit a mesogenic phase. Thus, one option for low MWIR absorption LCs is to reduce or shift the C–H absorptions away from the MWIR region. A short alkyl chain helps to lower the absorption loss but it often results in a high melting point, a narrow or even no mesogenic phase. Shifting the CH bond absorption to a longer wavelength seems to be a promising approach. The molecular vibration frequency ( $\omega$ ) depends on the spring constant ( $\kappa$ ) and reduced mass ( $\mu$ ) of the diatomic group as:

$$\omega = \sqrt{\kappa/\mu} \quad (1)$$

Therefore, as the reduced mass increases the vibration frequency decreases, *i.e.* the absorption band shifts towards a longer wavelength. According to this concept, several molecular design strategies have been proposed for shifting the absorption bands outside the MWIR region, such as: (1) deuteration,<sup>26</sup> (2) chlorination,<sup>27,28</sup> and (3) fluorination.<sup>29,30</sup> Deuteration shifts the CH vibration bands

<sup>a</sup> State Key laboratory of Fluorine & Nitrogen Chemicals, Xi'an 710065, China.

E-mail: gmecazw@163.com; Fax: +86 29 8153 0702; Tel: +86 29 88291846

<sup>b</sup> Xi'an Modern Chemistry Research Institute, Xi'an 710065, China

<sup>c</sup> College of Optics and Photonics, University of Central Florida, Orlando, Florida, USA

<sup>d</sup> School of Physical Electronics, University of Electronic Science and Technology of China, Chengdu, 610054, China

<sup>e</sup> Science of Technology on Electro-Optical Information Security Control Laboratory, Sanhe, 065201, China

† Electronic supplementary information (ESI) available: Synthesis and all characterization data. Tables S1 and S2, Fig. S1 and S2. See DOI: 10.1039/c6tc01249c

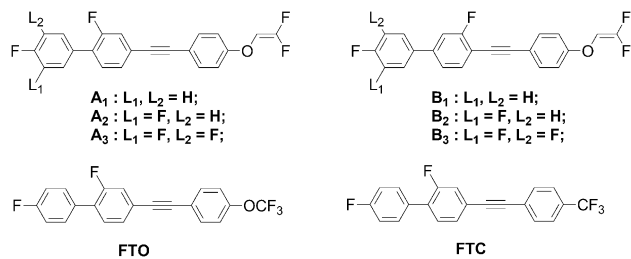


Fig. 1 Chemical structures of synthesized compounds and reference compounds **FTO** and **FTC**.

to a longer wavelength by a factor of  $\sqrt{2}$ , which unfortunately is still in the MWIR region. Therefore, a heavier atom is needed. Vibration bands of C–Cl occur in the 12.5–15.4  $\mu\text{m}$  region which seems to be a promising approach for IR LCs. However, the alkyl chain must be retained to preserve the nematic phase. As a result, the strong and broad C–H vibration absorption bands which occur in the 3.2–3.7  $\mu\text{m}$  region still exist. The vibration frequencies of CF, CF<sub>2</sub>, and CF<sub>3</sub> bonds occur in the 7–9  $\mu\text{m}$  region and fluorinated LCs have been widely used in active matrix LCDs.<sup>13</sup> In these compounds, the fluoro substitutions are mainly in the phenyl ring. The first LC compound with the perfluoro chain was reported by Chen *et al.* in 2011 and demonstrated a highly transparent window in the MWIR region.<sup>29</sup> However, due to the lack of flexibility, some undesired properties such as a narrow nematic range ( $\sim 2$  °C) and a high melting point (85.8 °C) appear, which hinder its practical application. Recently, our group reported a series of tolane liquid crystals with the trifluoromethoxy terminal group (**FTO**, Fig. 1), which exhibits not only high transparency in the MWIR region but also a wide nematic range (up to 81.8 °C).<sup>30</sup> Unfortunately their melting points are too high to formulate a room temperature LC mixture.

As a sequential approach to MWIR applications, two series of 2,2-difluorovinyl terminated tolane liquid crystals were designed and prepared, and their structures are shown in Fig. 1. Two compounds **FTO** and **FTC** were used for comparison and their synthesis methods have been reported elsewhere.<sup>30</sup> Moreover, a eutectic mixture was formulated using 2,2-difluorovinyl terminated tolane liquid crystals with a nematic phase at room temperature. Its physical properties such as MWIR transmittance, dielectric anisotropy, viscosity and birefringence were investigated.

## Experimental section

### Materials

1-Bromo-4-(2,2,2-trifluoroethoxy)benzene, 1-bromo-2-fluoro-4-iodobenzene and 1-bromo-3-fluoro-4-iodobenzene were purchased from Xi'an Caijing Opto-Electrical Science Technology Co. Ltd and used as received. All other chemical reagents used in this experiment were purchased from Sigma-Aldrich and were of analytical grade and used without further purification.

### Synthesis

The synthetic routes and general procedures of the compounds are illustrated in Scheme 1. Selective Sonogashira–Hagihara

coupling was predominant for the synthesis of the phenylethynyl tolane unit. Details of the synthesis, yields and characterization data can be found in the ESI†

## Results and discussion

### Synthesis and characterization

Novel 2,2-difluorovinyl-based tolane LCs were synthesized as shown in Scheme 1, including five-step reactions starting from 1-bromo-4-(trifluoromethoxy) benzene. All LCs were obtained with purities higher than 99.5% (GC and high performance liquid chromatography). The structures of the products were characterized by MS, <sup>1</sup>H-NMR and <sup>13</sup>C-NMR spectroscopy. All of these results confirmed the proposed structures of the target compounds.

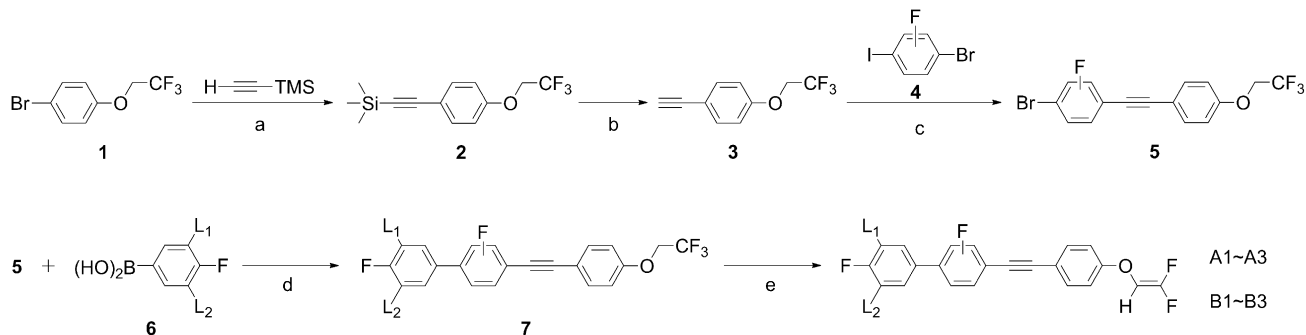
The crucial intermediate **5** was synthesized by a highly site-selective Sonogashira reaction. The site-selectivity depends on the reaction conditions and the nature of the substrates. By optimization of the reaction temperature to 0 °C and sequential loading of iodobenzene, high yields ( $\sim 80\%$ ) were obtained.

### Mesomorphic properties

The phase transition temperature and texture of the samples were acquired on the Mettler-Toledo FP82 HT hot stage combined with a FP90 controller and in conjunction with differential scanning calorimetry (DSC). The identification of the nematic mesophase of the compounds was made from the observation of the typical planar thread texture by polarizing optical microscopy (Olympus, BX51). The planar thread-like texture is a characteristic of the liquid-crystalline nematic phase.<sup>31</sup> For example, Fig. S1 (see ESI†) displays the typical thread-like texture of the nematic mesophase measured for **A1** in the heating process.

The transition temperature (°C) and heat fusion enthalpy ( $\text{kJ mol}^{-1}$ ) of the LC compounds were measured using a DSC (Mettler-Toledo DSC1) under nitrogen atmosphere at heating and cooling rates of 5 °C per minute. The phase transition temperatures reported here were the peak values of the transition on DSC curves. The results are summarized in Table 1 and the DSC curves are shown in the ESI† (see Fig. S2). The POM images and DSC thermograms show that **A1**, **A2**, **B1** and **B2** exhibit a stable nematic phase and a supercooling phenomenon was also observed (see Table 1). Additionally, for **A3** and **B3**, monotropic nematic phases were observed, respectively. For example, upon heating at 75.2 °C, **B3** converts directly into the isotropic phase, and upon cooling, the sample displays two peaks in DSC trace. These peaks were assigned to monotropic transitions  $I \rightarrow N$  at 76.7 °C and  $N \rightarrow C$  at 64.4 °C, respectively.

Fig. 2 shows how the position and number of fluorine atoms influence the phase properties of LCs. It is obviously shown that the mesomorphic intervals are decreased with the increase of lateral fluorine substitutions in both series. For instance, **A1** melts to the nematic phase at 61.3 °C and converts to the isotropic phase at 155.9 °C, with  $\Delta T = 94.6$  °C, but for **A2** the nematic phase range  $\Delta T = 38.5$  °C and **A3** exhibits only a monotropic nematic phase. Compared with series **B**, series **A**



**Scheme 1** Synthetic method for preparation of compounds **A1–A3** and **B1–B3**. (a) Pd(PPh<sub>3</sub>)<sub>2</sub>Cl<sub>2</sub>, Cul, Et<sub>3</sub>N, 70 °C. (b) KOH, EtOH, r.t. (c) Pd(PPh<sub>3</sub>)<sub>2</sub>Cl<sub>2</sub>, Cul, Et<sub>3</sub>N, 0 °C. (d) Pd(PPh<sub>3</sub>)<sub>4</sub>, TBAB, K<sub>2</sub>CO<sub>3</sub>, PhMe/EtOH/H<sub>2</sub>O, reflux. (e) LDA, THF, –70 °C.

**Table 1** Transition temperature (°C) and enthalpy values (kJ mol<sup>-1</sup>)

Entry	Transition temperature/°C (enthalpy change/kJ mol <sup>-1</sup> )	
	Heating process	Cooling process
<b>A1</b>	C <sub>1</sub> 59.3 (11.2) C <sub>2</sub> 61.3 (23.49) N 155.9 (0.48) I <sup>a</sup>	I 155.6 (0.44) N 28.8 (5.32) C <sub>2</sub> 21.6 (7.96) C <sub>1</sub>
<b>A2</b>	C 67.7 (21.62) N 106.2 (0.15) I	I 105.8 (0.27) N 31.2 (17.50) C
<b>A3</b>	C 51.23 (25.71) I	I 43.6 (0.05) N 9.8 (5.05) C
<b>B1</b>	C 88.2 (32.93) N 173.5 (0.33) I	I 173.1 (0.41) N 40.7 (12.6) C
<b>B2</b>	C 66.1 (22.75) N 126.2 (0.19) I	I 126.0 (0.23) N 46.5 (19.35) C
<b>B3</b>	C 75.2 (24.42) I	I 76.7 (0.07) N 64.4 (20.26) C
<b>FTO</b>	C 95.3 (30.09) N 137.4 (0.41) I	I 137.0 (0.45) N 17.2 (13.99) C
<b>FTC</b>	C 91.1 (24.76) I	I 85.3 (0.25) N 46.1 (6.41) C

<sup>a</sup> C<sub>1</sub>: crystal 1; C<sub>2</sub>: crystal 2; N: nematic mesophase; I: isotropic liquid.

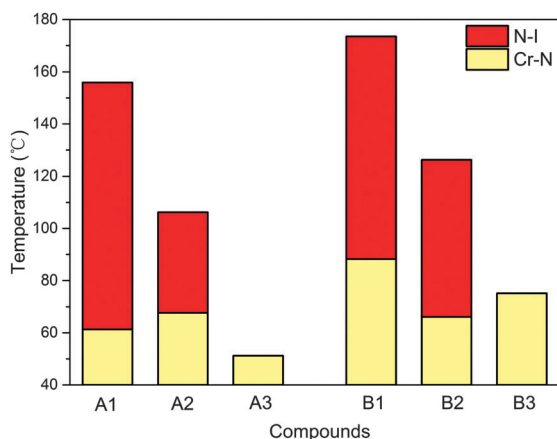


**Fig. 2** Mesophase range of **A** and **B** series during heating. C: crystal, N: nematic.

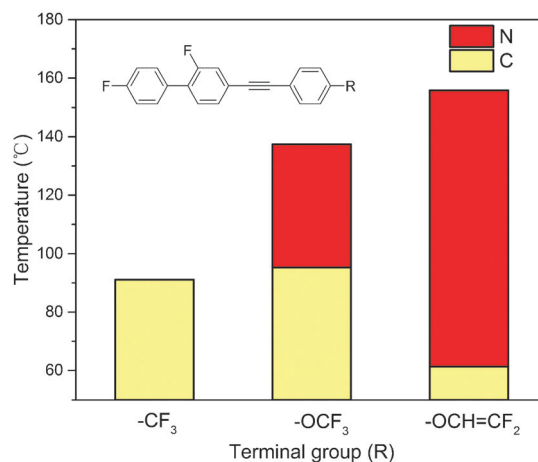


**Fig. 3** Mesophase range of compounds **A1**, **FTO**, and **FTC** during heating. C: crystal, N: nematic.

exhibits a lower melting point and a wider mesomorphic temperature range, which indicates that the lateral fluoro substitution on the central phenyl ring away from the triple bond is more helpful in enhancing the stability of the mesophase.

Fig. 3 illustrates how the terminal groups impact the phase properties of LCs with the same skeleton and fluorine atom. The new compounds with 2,2-difluorovinyl as the terminal group (**A1**) exhibit the highest clearing point and lowest melting point, compared to the analogues trifluoromethoxyl (**FTO**) and trifluoromethyl (**FTC**) terminal compounds. Since the previously reported

trifluoromethoxyl terminated LCs<sup>29</sup> suffer from a high melting point which hinders their application in the IR region, the new LCs with a low melting point are beneficial for formulating a room temperature eutectic mixture.

#### Mid-infrared absorption properties

Since the structures of synthesized compounds are very close, their absorption properties are also very similar.<sup>27</sup> Here we choose compound **A1** as a probe for testing MWIR absorption

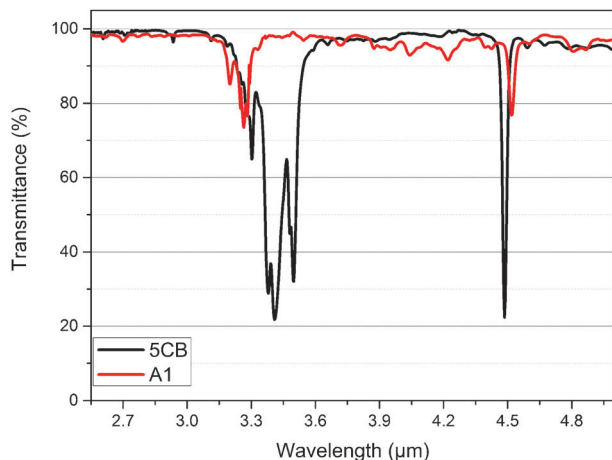


Fig. 4 Measured transmission spectra of **A1** (red) and **5CB** (black).

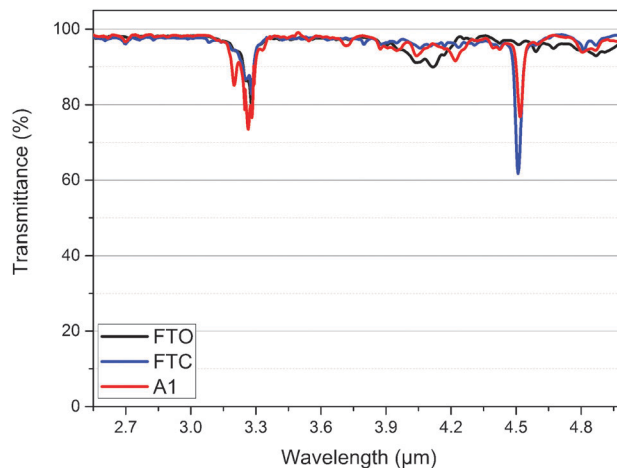


Fig. 5 Measured transmission spectra of **A1** (red), **FTO** (black), and **FTC** (blue).

properties. We also measured the MWIR properties of **5CB** (4-cyano-4'-pentylbiphenyl) as a benchmark and **FTO** and **FTC** for comparison. All the samples were dissolved in  $\text{CCl}_4$  at a concentration of  $5 \times 10^{-5} \text{ mol ml}^{-1}$  and then filled in a  $\text{CaF}_2$  IR cell with a gap of 0.5 mm. The measurement of MWIR transmission spectra was carried out on a Bruker FT-IR spectrometer. The transmission spectra of the compounds were normalized to that of  $\text{CCl}_4$ .

As illustrated in Fig. 4, **5CB** exhibits a quite broad and strong absorption around  $\lambda = 3.4 \mu\text{m}$  which ascribed to the C–H stretching. The  $\text{C}\equiv\text{N}$  stretching band shows a sharp and strong absorption which occurs at  $\lambda = 4.48 \mu\text{m}$ . **A1** shows a much weaker and narrower absorption in the vicinity of  $3.3 \mu\text{m}$ , which confirms that the unsaturated C–H bonds [e.g. Ar C–H, vinyl C–H] have a much weaker and narrower absorption near  $\lambda = 3.4 \mu\text{m}$  than that of the saturated C–H bonds [e.g. alkyl C–H]. The absorption peak at  $3.28 \mu\text{m}$  originates from the CH vibration in the phenyl ring and the vinyl bond. The fairly weak absorption at  $\sim 4.2 \mu\text{m}$  results from the C–O and C–F combination overtone. Compared to the strong  $\text{C}\equiv\text{N}$  absorption at  $4.48 \mu\text{m}$ , the  $\text{C}\equiv\text{C}$  vibration (at  $4.52 \mu\text{m}$ ) is much weaker.

Fig. 5 illustrates the absorption properties of LCs that have the same skeleton and fluorine atom but different terminal groups. Overall speaking, these three compounds all exhibit relatively high transmittance in the  $2.7\text{--}5 \mu\text{m}$  region. **A1** shows a slightly broader and stronger absorption in the vicinity of  $3.3 \mu\text{m}$ , which is attributed to the vinyl CH bond. **FTO** exhibits the lowest  $\text{C}\equiv\text{C}$  absorption at  $4.5 \mu\text{m}$ , followed by **A1** and then **FTC**. This character could potentially be due to the molecular symmetrical changes with terminal groups. We observe that the absorption at  $\sim 4.2 \mu\text{m}$  decreases when the terminal group alternates from  $-\text{OCF}_3$  to  $-\text{OCH}=\text{CF}_2$ , and then  $-\text{CF}_3$ . It means that the absorption of  $4.2 \mu\text{m}$  mainly originates from C–O stretching vibrations and is enhanced by C–F vibrations.

### Physical properties

Table 2 summarizes the measured birefringence ( $\Delta n$ ), viscosity ( $\gamma_1$ ) and dielectric anisotropy ( $\Delta\epsilon$ ) of all these compounds. A guest–host

Table 2 Measured birefringence ( $\Delta n$ ), dielectric anisotropy ( $\Delta\epsilon$ ), viscosity ( $\gamma_1$ ) and calculated molecular polarizability anisotropy  $\Delta\alpha^b$  of synthesized compounds, **FTO** and **FTC**

Compound	$\Delta\alpha^a$	$\Delta n^b$	$\Delta\epsilon^b$	$\gamma_1^b$
<b>A1</b>	394.7	0.3294	1.38	96.3
<b>A2</b>	392.7	0.3127	2.28	114.6
<b>A3</b>	391.5	0.2997	5.59	123.2
<b>B1</b>	400.2	0.3339	1.04	82.8
<b>B2</b>	398.1	0.3169	0.24	98.5
<b>B3</b>	397.8	0.3028	2.50	102.5
<b>FTO</b>	350.7	0.2875	0.64	77.4
<b>FTC</b>	331.5	0.2851	1.35	96.6

<sup>a</sup> The polarizability anisotropy parameters are expressed in Bohr<sup>3</sup> (with 1 Bohr = 0.52917 Å) <sup>b</sup> Measured results.

method was used by doping 10 wt% of each compound to a host mixture (**CJOE-001**, for compositions and properties see Table S1 in the ESI†). The  $\Delta n$  values were measured by using an Abbe refractometer at  $\lambda = 589 \text{ nm}$  and  $T = 25 \text{ }^\circ\text{C}$ ,  $\Delta\epsilon$  using an electrical constant instrument (EC-1, TOYO Corporation, Japan) and  $\gamma_1$  using a Model 6254 (Multi Channel Liquid Crystal Evaluation System, TOYO Corporation, Japan) at  $T = 25 \text{ }^\circ\text{C}$ .

As shown in Table 2, both **A** and **B** series possess a relatively high birefringence ( $\Delta n > 0.30$ ). It is clearly shown that the more fluoro substitutions in the phenyl ring, the lower the birefringence. For example,  $\Delta n = 0.3339$  for compound **B1**, but it gradually decreases to 0.3169 for **B2** and 0.3028 for **B3** with the increased fluoro substitution (see Table 2). Meanwhile, series **B** exhibits a higher birefringence than series **A**, which indicates that the lateral fluoro substitution on the central phenyl ring toward the triple bond is more helpful in enhancing the birefringence. The main reason is that the biphenyl moiety in series **A** is less coplanar than in series **B** due to the existence of lateral fluoro substitution.

Comparing the compounds with the same skeleton and fluorine atom but different terminal groups (**A1**, **FTO** and **FTC**), the 2,2-difluorovinyl terminal compounds lead to the highest  $\Delta n$ , from 0.3294 for **A1**, 0.2875 for **FTO** and 0.2851

for **FTC**, respectively. These results are expected because the 2,2-difluorovinyl group increases the conjugation of the molecules.

On the molecular level, the magnitude of the birefringence strongly depends on the molecular polarizability anisotropy  $\Delta\alpha$  for elongated molecules.<sup>32</sup> Modification of the molecular structure can affect the  $\Delta\alpha$  and finally lead to the change in the  $\Delta n$  value. We used molecular simulation program Gaussian 09<sup>33</sup> to calculate the molecular polarizabilities. Details of the procedure have been reported elsewhere.<sup>32</sup> The calculated data are also listed in Table 2. The calculated results of molecular polarizabilities are in good agreement with the measured  $\Delta n$  values. For instance, series **B** possesses a higher  $\Delta\alpha$  than that of series **A** (e.g.  $\Delta\alpha = 400.2$  for **B1** and  $\Delta\alpha = 394.7$  for **A1**), which explains why series **B** exhibits a higher  $\Delta n$  than that of series **A**. Meanwhile, comparing compounds **A1** with **FTO** and **FTC**, the  $\Delta\alpha$  value decreases from 394.7 to 350.7 and then 331.5, accordingly the  $\Delta n$  decreases from 0.3294 to 0.2875 and then 0.2851 (Table 2). Thus, introducing more polarizable terminal groups can effectively enhance the molecular polarizability anisotropy, thereby enhancing the birefringence.

High birefringence is a crucial requirement for IR applications. The total phase change ( $\delta$ ) of an LC device is governed by the following equation:

$$\delta = 2\pi d\Delta n/\lambda \quad (2)$$

where  $d$  is the cell gap,  $\Delta n$  is the LC birefringence and  $\lambda$  is the wavelength. From eqn (2), the phase shift decreases as the wavelength increases. Thus, to get a  $2\pi$  phase change for a longer wavelength, the required  $d\Delta n$  should increase proportionally. Moreover, as the wavelength increases, the LC birefringence gradually decreases and then saturates in the near IR region. Thus, our new high  $\Delta n$  LCs enable a thin cell gap to be employed for achieving two important objectives: (1) lower absorption loss, and (2) faster response time.

Since these compounds have dipoles on both terminal groups and their dipole moments almost cancel each other, a small to moderate  $\Delta\epsilon$  (between 0.24 and 5.59) was observed. The  $\Delta\epsilon$  value of series **A** increases as the lateral fluorine substitution increases, while that of series **B** first decreases (**B2**) and then increases (**B3**). Compound **B2** shows the lowest value of  $\Delta\epsilon$ , which implies that the dipole moments on both sides are almost equal. Another key performance parameter is viscosity. As shown in Table 2, all of these compounds exhibit a relatively low viscosity. The viscosity gradually increases with the increasing lateral fluorine substitutions in both series. That can be easily understood because a bulkier compound often exhibits a higher viscosity.

### Eutectic mixture

An LC mixture with a nematic phase at room temperature is highly desirable for practical application.<sup>34</sup> To lower the melting point, a eutectic mixture was formulated according to the Schroder-van Laar equation, designated as **IR01**, using our synthesized compounds (for compositions of the mixture, see Table S2 in the ESI†).

DSC was used to measure the thermal properties of **IR01**. The measured melting point was 12.3 °C and the clearing point was 102.8 °C during the heating process (for the DSC curve, see Fig. S2 in the ESI†). The melting point decreased to below -20 °C upon super-cooling. This result proves that a room temperature mixture is thus obtained by using the synthetic liquid crystals with the 2,2-difluorovinyl terminal group. The dielectric anisotropy and viscosity of the mixture were measured at room temperature and found to be  $\Delta\epsilon = 2.37$  ( $\epsilon_{\parallel} = 7.35$ ,  $\epsilon_{\perp} = 4.98$ ) and  $\gamma_1 = 182.9$  mPa s. Such a low viscosity is beneficial for fast response time.

To determine the birefringence in the IR region, we measured the dispersion curve using a multi-wavelength Abbe refractometer at  $\lambda = 486, 546, 589$  and  $656$  nm and  $T = 25$  °C. The results are plotted in Fig. 6. The dots are measured data at different wavelengths and the solid line is the fitting curve obtained using the single band model:<sup>35</sup>

$$\Delta n(\lambda) = G \frac{\lambda^2 \cdot \lambda^{*2}}{\lambda^2 - \lambda^{*2}} \quad (3)$$

where  $G$  is a proportionality constant and  $\lambda^*$  is the mean resonance wavelength. Through fitting, we obtained  $G = 3.89 \mu\text{m}^{-2}$  and  $\lambda^* = 0.255 \mu\text{m}$ . Based on these parameters, the birefringence at any wavelength can be obtained. As shown in Fig. 6, the  $\Delta n$  value decreases as  $\lambda$  increases and then reaches a plateau. For **IR01**, its birefringence remains relatively high ( $\Delta n \approx 0.254$ ) at  $\lambda = 4 \mu\text{m}$ . Based on eqn (2), to achieve a  $2\pi$  phase change at  $\lambda = 4 \mu\text{m}$ , the required cell gap is about 16  $\mu\text{m}$ .

The absorption coefficient ( $\alpha$ ) at discrete wavelengths was obtained by filling **IR01** in a  $\text{CaF}_2$  IR cell with a cell gap of  $\sim 50 \mu\text{m}$  and the cell was heated to an isotropic state to avoid light scattering. To take surface reflections into consideration, we used a single  $\text{CaF}_2$  crystal as the reference. The measured results are plotted in Fig. 7. The absorption spectrum of **5CB** is also included for comparison, which can be found in ref. 27 and 29. From Fig. 7, **IR01** exhibits a much lower absorption in the MWIR region. For example, **IR01** exhibits a transparent

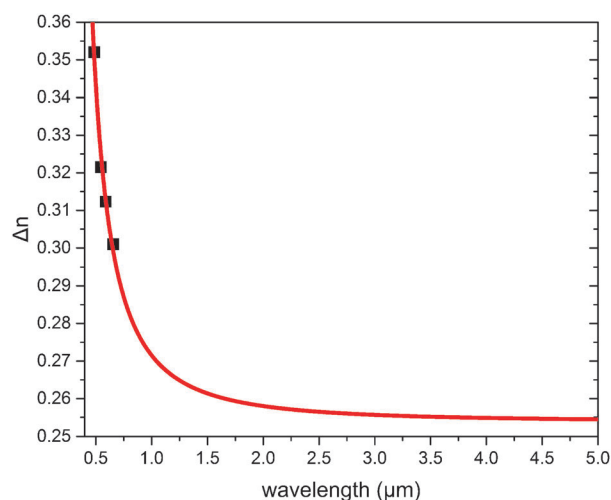


Fig. 6 Birefringence dispersion of **IR01** at  $T = 25$  °C: The dots are measured data and the solid line is fitted with eqn (3).

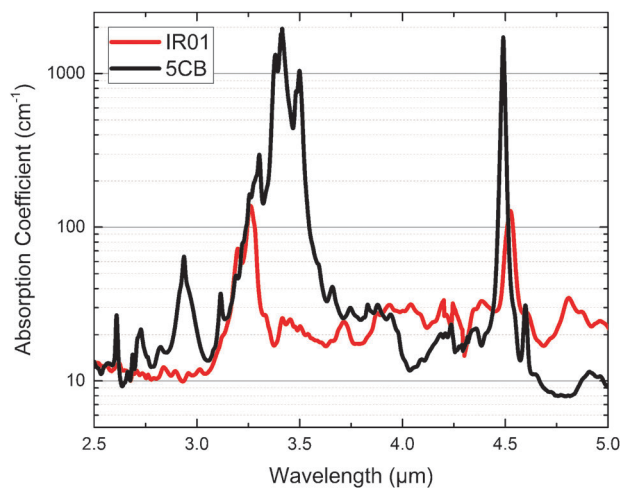


Fig. 7 Measured absorption coefficient spectra of 5CB and IR01.

window from 2.5  $\mu\text{m}$  to 3.1  $\mu\text{m}$ , the corresponding baseline absorption coefficient is around  $10\text{ cm}^{-1}$ . More importantly, the absorption of IR01 at 3.1–3.6  $\mu\text{m}$  is much smaller and narrower than that of 5CB. For instance, the highest absorption peak of IR01 occurs at 3.27  $\mu\text{m}$  and the absorption coefficient is  $137\text{ cm}^{-1}$ , while the highest absorption peak of 5CB appears at 3.41  $\mu\text{m}$  and the absorption coefficient is  $1960\text{ cm}^{-1}$ . The transmittance of a scattering-free LC device is governed by:

$$T = \exp(-\alpha d) \quad (4)$$

where  $d$  is the cell gap. If we use a 16  $\mu\text{m}$  cell to achieve a  $2\pi$  phase, the transmittance of IR01 is higher than 80%, but the transmittance of 5CB is lower than 5%.

## Conclusions

Low absorption loss, a wide nematic range and high birefringence are crucial requirements for liquid crystals used in the MWIR region. In this work, two sets of tolane liquid crystal materials terminated by 2,2-difluorovinyl group were synthesized and characterized. Their mesophase properties, birefringence ( $\Delta n$ ) and MWIR absorption properties were examined. The 2,2-difluorovinyl terminal group provides a wider nematic phase range, lower melting point and high birefringence, along with low absorption loss. Additionally, a eutectic mixture was formulated, which exhibits a nematic phase from room temperature to over 100  $^{\circ}\text{C}$ . The mixture shows a high birefringence ( $\Delta n = 0.254$ ) at  $\lambda = 4\text{ }\mu\text{m}$ , moderate dielectric anisotropy ( $\Delta\epsilon = 2.37$ ), reasonably low viscosity ( $\eta_1 = 182.9\text{ mPa s}$ ) and low absorption loss in some windows in the 3–5  $\mu\text{m}$  region. All of these characteristics demonstrate that this mixture is an outstanding candidate for both amplitude and phase modulations in the MWIR region.

## Acknowledgements

The Xi'an group is indebted to the Defence Industrial Technology Development Program of China (B0520132007, B1120132028).

## Notes and references

- H. Wang, L. Wang, H. Xie, C. Li, S. Guo, M. Wang, C. Zou, D. Yang and H. Yang, *RSC Adv.*, 2015, **5**, 33489–33495.
- Y. Gao, W. Yao, J. Sun, H. Zhang, Z. Wang, L. Wang, D. Yang, L. Zhang and H. Yang, *J. Mater. Chem. A*, 2015, **3**, 10738–10746.
- S. T. Wu, U. Efron and L. D. Hess, *Appl. Phys. Lett.*, 1984, **44**, 1033–1035.
- Z. Cheng, T. Wang, X. Li, Y. Zhang and H. Yu, *ACS Appl. Mater. Interfaces*, 2015, **7**, 27494–27501.
- P. Yaghmaee, O. H. Karabey, B. Bates, C. Fumeaux and R. Jakoby, *Int. J. Antenn. Propag.*, 2013, **24**, 1456–1459.
- V. Urruchi, C. Marcos, J. Torrecilla, J. M. Sánchez-Pena and K. Garbat, *Rev. Sci. Instrum.*, 2013, **84**, 026102.
- M. Reuter, K. Garbat, N. Vieweg, B. M. Fischer, R. Dąbrowski, M. Koch, J. Dziaduszek and S. Urban, *J. Mater. Chem. C*, 2013, **1**, 4457–4463.
- L. Wang, X. Lin, W. Hu, G. Shao, P. Chen, L. Liang, B. Jin, P. Wu, H. Qian, Y. Lu, X. Liang, Z. Zheng and Y. Lu, *Light: Sci. Appl.*, 2015, **4**, e253.
- R. Soref, *Nat. Photonics*, 2010, **4**, 495–497.
- D. Ouzounov and F. Freund, *Adv. Space Res.*, 2004, **33**, 268–273.
- B. Kuyken, X. Liu, R. Osgood Jr., R. Baets, G. Roelkens and M. J. Green, *Opt. Express*, 2011, **19**, 20172–20181.
- S. Kurata and T. Nagatani, *Physica A*, 2015, **81**, 29.12.1.
- T. Geelhaar, K. Griesar and B. Reckmann, *Angew. Chem., Int. Ed.*, 2013, **52**, 8798–8809.
- J. Li, S. T. Wu, S. Brugioni, R. Meucci and S. Faetti, *J. Appl. Phys.*, 2005, **97**, 073501.
- P. F. McManamon, T. A. Dorschner, D. L. Corkum, L. J. Friedman, D. S. Hobbs, M. Holz, S. Liberman, H. Q. Nguyen, D. P. Resler and R. C. Sharp, *Proc. IEEE*, 1996, **84**, 268–298.
- S. Xu, H. Ren and S. T. Wu, *Opt. Express*, 2012, **20**, 28518–28523.
- S. Mitsunori and H. Keisuke, *Opt. Express*, 2013, **21**, 11984–11993.
- J. W. Mccargar, R. Ondris-Crawford and J. L. West, *J. Electron. Imaging*, 1992, **1**, 22–28.
- L. Scolari, L. Wei, S. Gauza, S. T. Wu and A. Bjarklev, *Opt. Rev.*, 2011, **18**, 114–116.
- S. T. Wu and R. J. Cox, *Liq. Cryst.*, 1989, **5**, 1415–1424.
- S. T. Wu, *J. Appl. Phys.*, 1998, **84**, 4462–4465.
- H. Sun, F. Roussel, W. S. Cheung, B. M. Fung, S. S. Keast, M. Lohman, J. Kim and M. E. Neubert, *Liq. Cryst.*, 2001, **28**, 1483–1486.
- S. T. Wu, C. S. Hsu and Y. Y. Chuang, *Jpn. J. Appl. Phys.*, 1999, **38**, L286–L288.
- C. S. Hsu, K. F. Shyu, Y. Y. Chuang and S. T. Wu, *Liq. Cryst.*, 2000, **27**, 283–287.
- S. T. Wu and K. C. Lim, *Appl. Opt.*, 1987, **26**, 1722–1727.
- S. T. Wu, Q. H. Wang, M. D. Kempe and J. A. Kornfield, *J. Appl. Phys.*, 2002, **92**, 7146–7148.
- F. Peng, Y. Chen, S. T. Wu, S. Tripathi and R. J. Twieg, *Liq. Cryst.*, 2014, **41**, 1545–1552.

- 28 F. Peng, D. Xu, H. Cheng and S. T. Wu, *Opt. Express*, 2015, **23**, 2361–2368.
- 29 Y. Chen, H. Xiangyu, J. Sun, P. Kula, D. Roman, S. Tripathi, R. J. Twieg and S. T. Wu, *Opt. Express*, 2011, **19**, 10843–10848.
- 30 M. Hu, Z. An, J. Li, L. Mo, Z. Yang, J. Li, Z. Che and X. Yang, *Liq. Cryst.*, 2014, **41**, 1696–1702.
- 31 I. Dierking, *Textures of Liquid Crystals*, Wiley-VCH, Weinheim, 2004, pp. 51–54.
- 32 R. Chen, Y. Jiang, J. Li, Z. An, X. Chen and P. Chen, *J. Mater. Chem. C*, 2015, **3**, 8706–8711.
- 33 M. J. Frisch, G. W. Trucks, H. B. Schlegel, G. E. Scuseria, M. A. Robb, J. R. Cheeseman, G. Scalmani, V. Barone, B. Mennucci, G. A. Petersson, H. Nakatsuji, M. Caricato, X. Li, H. P. Hratchian, A. F. Izmaylov, J. Bloino, G. Zheng, J. L. Sonnenberg, M. Hada, M. Ehara, K. Toyota, R. Fukuda, J. Hasegawa, M. Ishida, T. Nakajima, Y. Honda, O. Kitao, H. Nakai, T. Vreven, J. A. Montgomery Jr, J. E. Peralta, F. Ogliaro, M. Bearpark, J. J. Heyd, E. Brothers, K. N. Kudin, V. N. Staroverov, R. Kobayashi, J. Normand, K. Raghavachari, A. Rendell, J. C. Burant, S. S. Iyengar, J. Tomasi, M. Cossi, N. Rega, J. M. Millam, M. Klene, J. E. Knox, J. B. Cross, V. Bakken, C. Adamo, J. Jaramillo, R. Gomperts, R. E. Stratmann, O. Yazyev, A. J. Austin, R. Cammi, C. Pomelli, J. W. Ochterski, R. L. Martin, K. Morokuma, V. G. Zakrzewski, G. A. Voth, P. Salvador, J. J. Dannenberg, S. Dapprich, A. D. Daniels, Ö. Farkas, J. B. Foresman, J. V. Ortiz, J. Cioslowski and D. J. Fox, *GAUSSIAN 09(Revision B.01)*, Gaussian Inc., Wallingford, CT, 2010.
- 34 M. Hird, *Chem. Soc. Rev.*, 2007, **36**, 2070–2095.
- 35 S. T. Wu, *Phys. Rev. A: At., Mol., Opt. Phys.*, 1986, **33**, 1270–1274.